Value of Resilience for Self-Sustained Highway Transportation Systems

Xuan Liu, *Student Member, IEEE,* Haoyuan Yan, *Student Member, IEEE,* Zhanglei Guan, *Student Member, IEEE,* Debin Zeng, *Student Member, IEEE,* Chenghong Gu, *Senior Member, IEEE,* Tianyang Zhao, *Senior Member, IEEE*

***Abstract*—Nowadays, self-sustained highway transportation systems (HTSs) are calling for the inter-operation of road networks, distribution networks (DNs), and electric vehicles (EVs) towards the unexpected impacts inducted by extreme weather events (EWEs). A novel joint resilience assessment scheme is proposed to quantify the resilience of self-sustained HTSs under tropical cyclone (TC) events. The impacts of TCs on transmission lines and highways are formulated using a two-step ambiguity set. In the first step, a multitask learning (MTL) based model with a novel training strategy is proposed to simulate the future TC tracks; the impacts of TCs are then calculated in the second step based on the simulation results. Using the ambiguity set, the self-sustained HTSs resilience assessment problem is formulated based on the dynamic optimal traffic assignment problem, where EVs are integrated as third-party emergency resources before the advent of TCs. This scheme is then formulated as a two-stage distributionally robust optimization (DRO) problem and reformulated as a mixed-integer programming (MILP) problem. Case studies have been conducted on a self-sustained HTS consisting of a modified IEEE-14 bus test system with 2 wind farms (WFs) and a 14-node transportation network with 4 charging stations (CSs). Numerical results indicate that the proposed scheme can quantify the resilience of self-sustained highway transportation systems under the joint operation of EVs and MGs regarding the unmet travel demand and load-shedding costs. In comparison to the statistical TC forecasting models, the proposed MTL-based model is more accurate and can reduce the system cost in most cases.**

***Index Terms*—Electric vehicles, networked microgrids, resilience, self-sustained.**

NOMENCLATURE

Main parameters and variables are explained in this nomenclature. The rest of them are defined when needed.

A. Indexes

d	Index of demand
g	Index of generators
w	Index of wind farms
s	Index of destinations
a	Index of links
t	Index of time periods
c	Index of EV classes
e	Index of energy levels for EVs

B. Sets

$\mathcal{D}$	Set of demand
$\mathcal{G}$	Set of generators
$\mathcal{W}$	Set of wind farms
$\mathcal{N}_S$	Set of source node
$\mathcal{A}$	Set of arcs
$\mathcal{A}_S$	Set of sink arcs
$\mathcal{T}$	Set of time periods
$\mathcal{C}$	Set of EV classes
$\mathcal{E}_c$	Set of energy levels for EVs belonging to class c

C. Parameters

f_{TT}	Travel cost
f_g	Fuel cost of generator g
f_g^{R}	Spinning reserve cost of generator g
$f_g^{r,+}, f_g^{r,-}$	Regulation up/down cost of generator g
f_{VOUD}	Cost of unmet traffic demand
f_{VOLL}	Cost of load loss
f_{VOGC}	Cost of generation curtailment
f_{VOWC}	Cost of wind power curtailment
β_a	Travel time required by the backward shock wave from the exit to the entry of link a
B_{ij}	Reciprocal of reactance of line (i, j)
t_a	Free-flow travel time on link a
δ	Time period length

D. First-stage Variables

$U_{a,c}^{s,e}(t), V_{a,c}^{s,e}(t)$	Cumulative number of EVs of class c with energy level e that enter and leave link a to destination s during period t
$P_{ij}(t), P_{ji}(t)$	Power flow from bus i to j and j to i during period t
$P_g(t)$	Energy set-point of generator g during period t
$P_w(t)$	Power output of wind farm w during period t
$P_c^{\text{ev}}(t)$	Cumulative charging/discharging power of EVs of class c from/to the power network
P_a^{ev}	Charging power of link a
$I_{ij}(t)$	Binary variable. 1 if line (i, j) is online during period t, 0 otherwise
$R_g(t)$	Spinning reserve of generator g during period t
$r_g^+(t), r_g^-(t)$	Regulation up/down reserve of generator g during period t
$P_d(t)$	Power demand of load d during period t

E. Second-stage Variables

$u^{s,e}_{a,c}(t), v^{s,e}_{a,c}(t)$	Cumulative number of EVs of class c with energy level e that enter and leave link a to destination s during period t
$p^{\text{ev}}_c(t)$	Cumulative charging/discharging power of EVs of class c from/to the power network
p^{ev}_a	Charging power of link a
$D^{\text{ud}}_{a,s}(t)$	Unmet traffic demand during period t
$D_{a,s}(t)$	Predicted traffic demand during period t
$p^{\text{ls}}_d(t)$	Load shedding of load d during period t
$p^{\text{gc}}_g(t)$	Curtailment of generator g during period t
$p^{\text{wc}}_w(t)$	Curtailment of wind farm w during period t
$\gamma_i(t)$	Bus angle at bus i during period t
$I_{ij}(t)$	Binary variable. 1 if line (i,j) is online during period t, 0 otherwise

I. Introduction

ONGOING transportation electrification is strengthening the interaction between highway transportation systems (HTSs) and coming low-carbon distribution systems, with the increasing penetration of electric vehicles (EVs). The implementation of self-sustained HTSs has shown to be effective in reducing the consumption of fossil fuels and emissions of greenhouse gas [1]. However, in many regions of the world, HTSs are exposed to and suffer from extreme weather events (EWEs), such as tropical cyclones (TCs). Additionally, there is increasing evidence that the intensity and frequency of EWEs are increasing in the coming years [2], [3]. Under EWEs, HTSs should be properly incorporated into the joint emergency management schemes as self-sustained systems, providing emergency transportation and power supply to critical users. In order to guide emergency planning, it is necessary to assess the resilience of HTSs before the advent of EWEs, considering the inter-operation of power systems and transportation systems under emergencies. Due to the uncertain nature of EWEs and their impacts, it is challenging to conduct a proactive resilience assessment.

In this work, the concern for EWEs is emphasized on TC events, which come with extremely strong winds and precipitations. TCs can cause great disruptions not only to the transportation system, but also power distribution facilities in coastal areas [4]. To assess the impact of TCs, the distributions of several TC-related parameters (such as wind speed or pressure) at given locations need to be obtained by sampling from probabilistic TC simulation models. The TC simulation models can be divided into four categories: statistical, dynamic, ensemble, and deep learning models. Dynamical and ensemble models provide more accurate simulations, but are too time-consuming to run since the dynamical models require supercomputers to process the equations governing the physics [5] and motion of the atmosphere while the ensemble models often combine the results of multiple dynamical models to produce a better quality result [6]. On the other hand, statistical and deep learning models are more light-weighted but less accurate. In a resilience assessment problem, where a massive amount of simulations needs to be generated to properly capture the uncertainty of TC events, statistical and deep learning models are more applicable than the other two types of models. The early probabilistic TC simulation models were based on single site observation data [7], [8]. Different statistical distributions were used in this type of model to generate site-specific TC parameters, such as central pressure, translation speed, and heading angle, for Monte Carlo sampling. Due to the lack of data, the tail shape of these distributions could not be accurately estimated. In 2000, Vickery et al. [9] introduces the TC track model which generates TC-related parameters along the TC tracks. Since then, many works have been made to improve the track model [10], [11]. In recent years, deep learning-based TC track models have been developed [12] for TC simulations. Combined with mixture models, deep learning models are able to make conditional probabilistic predictions of TC tracks and intensities [13]. Deep learning models, once properly trained, generally perform better than statistical models [14]. However, deep learning models are extremely sensitive to hyperparameters that are hard to tune manually.

The modeling of TC impacts on HTSs and distribution networks (DNs) mainly focuses on characterizing the effect of weather conditions on the reliability attributes of HTSs and DNs, i.e. line failures, road capacities, and free-flow travel speeds. The distributions of these attributes during TC events are primarily affected by the wind speed, rainfall rates, and water film depth (WFD), which can be obtained by combining the probabilistic TC track models with statistical or empirical precipitation [15], wind field [16] and WFD [17] models. For DNs, TC-induced line failures are often simulated using the fragility curve of individual DN components, namely towers [18] and conductors [19]. Subsequently, failure probabilities of the distribution lines can be obtained by combining the failure models of its components. For HTSs, studies show that the free-flow travel time and road capacity of the inundated road segments are affected by the rainfall intensity and WFD during TC events [20], [21]. Ni et al. [21] suggest that the free-flow travel time and road capacity models based on Del Castillo model fit best for the observed traffic data.

For emergency management of HTSs, the dynamic traffic assignment model is widely adopted in transportation planning during a TC event [22]. Considering the uncertainties of traffic demand and flow constraints, a cell transmission model (CTM) based dynamic traffic assignment problem is proposed as a two-stage chance-constrained distributionally robust problem [23]. However, large-scale variables are introduced in the CTM model, making it difficult to solve the problem, especially considering uncertainties. The authors in [24] propose the link transmission model (LTM) to reduce the scale of variables. However, the energy characteristic of EVs has not been considered. Based on the LTM, a novel dynamic traffic assignment model is presented for the emergency reconfiguration where both gasoline vehicles and EVs are considered [22]. Overall, the resilience of power systems has yet to be considered in these works, while the self-sustained HTSs may be impacted by power shortage. Considering the cascading failure propaga-

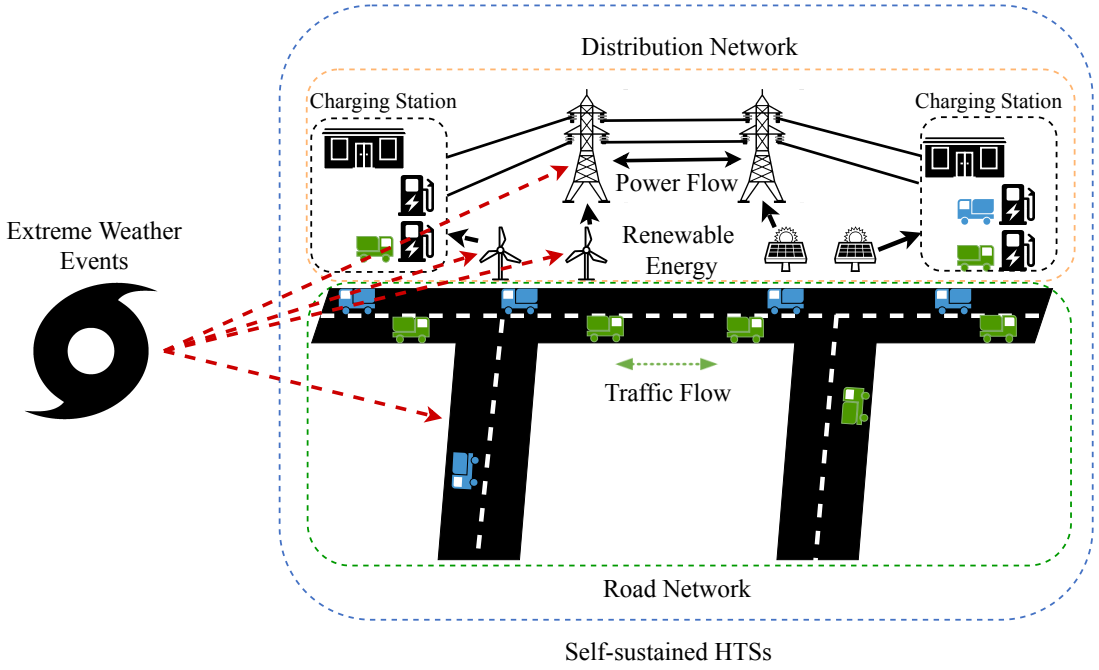

Fig. 1. Illustration of the resilience management scheme for self-sustained HTSs.

tion, an N-2 constraint economic dispatch model is developed to decrease the generation cost and load shedding [25]. To reduce the generation cost and deal with the wind power uncertainty, a two-stage adaptive robust economic dispatch model is proposed and is solved by a Benders decomposition method [26]. A two-stage economic dispatch model is formulated based on the distributionally robust optimization technique in [27] to minimize the generation cost and curtailment. However, the interaction of EVs in HTSs is ignored in these works.

To fulfill the research gaps on the proactive resilience assessment of HTSs considering self-sustaining, a novel resilience assessment scheme is proposed under the joint operation of EVs. Deep learning-based probabilities TC track models with automatic hyperparameter searching schemes are employed for the impact modeling of EWEs. The main contributions of this paper can be summarized as follows:

(1) A probabilistic TC simulation model based on multi-task learning (MTL) and mixture models is developed. To efficiently train the proposed model, a novel automatic hyperparameter tuning strategy is proposed. The impacts of TCs on distribution networks and HTSs are quantified using a series of empirical and analytical models based on the TC track simulation results.

(2) A two-stage distributionally robust optimization problem is formulated to quantify the resilience of HTSs under uncertain EWEs. The value of proactive resilience assessment with more accurate EWE predictions and EVs as a mobile energy source is examined by extensive case studies.

The remainder of the paper is organized as follows: Section II gives an overview of the resilience management of self-sustained HTSs. The proposed TC simulation model and TC impact modeling strategy are presented in Section III. Section IV introduces the resilience assessment problem of self-sustained HTS and the solution method. The proposed approach is validated through case studies in section V. Conclusions are drawn in sectionVI.

II. Resilience Management of Self-Sustained HTSs

A. Self-Sustained HTSs

Traditional HTSs rely on fossil fuels to power vehicles and facilities along the roads. As a consequence, the transportation sector has been one of the main contributors to greenhouse gas emissions in many countries [28], [29]. In recent years, self-sustained transportation systems have been introduced to reduce the dependency on fossil fuels and emissions of greenhouse gas. Implementing self-sustained HTSs has been one of the main objectives in the transition from fossil fuels to renewable energy sources. According to [30], self-sustained transportation systems should be equipped with polymorphic renewable energy sources, such as solar and wind, and be able to convert between different types of energies, such as thermal, electrical, and hydrogen energy. In such systems, the road networks, and DNs work together to meet the self-sustained energy supply and consumption goal. In addition, the traffic demand can be fulfilled by EVs powered by renewable energy, further reducing the demand for fossil fuels.

B. Resilience Management Scheme

To reduce the economic losses (e.g., load shedding and unmet traffic demands) of self-sustained HTSs under uncertain EWEs, a resilience management scheme is formulated based on the economic dispatch model. The impact of uncertain EWEs, which includes the failures of distribution lines, reduction of free-flow travel speed and road capacity, and change of

wind farm power output, can be simulated using probabilistic forecasting models. With the uncertain impact as the ambiguity set, the reconfiguration and generation of DNs, and the travel and charging of EVs are jointly optimized using a two-stage DRO model. Fig. 1 gives an overview of the self-sustained HTSs resilience management scheme.

III. Uncertain TC Simulation and Impact Modeling for Self-Sustained HTSs

A. Problem Definition

Definition 1: A *TC track* T is composed of N_T consecutive spatial-temporal points $T = \{X_1, X_2, ..., X_{N_T}\}$. Each spatial-temporal point X_i contains several parameters that essentially characterize the TC track at time step i: $X_i = [\lambda_i, \phi_i, p_{ci}]$, where λ_i, ϕ_i are the longitude and latitude coordinates of the TC center, and p_{ci} is the minimum TC central pressure.

Definition 2: A *power distribution network* D is denoted as a set of N_D transmission lines $D = \{L_0, L_1, ..., L_{N_D}\}$. Each transmission line L_i contains its own set of transmission towers and conductors. The *status of a transmission network* at any given time during a TC event can be represented by a binary vector of length N_D, where the status of each L_i is represented by a binary variable (0 = failure and 1 = online).

Definition 3: A *road network* R is denoted as a set of N_R road segments $D = \{S_0, S_1, ..., S_{N_R}\}$. Each road segment S_i is characterized by its starting and ending positions. The *status of a road network* at any given time during a TC event can be represented by a N_R by 2 matrix, where the ith row of the matrix represents the road capacity and free-flow travel speed of S_i.

Problem 1: Given a power distribution network D, a road network R, and a TC track $T = \{X_0, X_1, ..., X_4\}$ that contains the past 24-hour track information, the goal is to predict the probability distribution of the status of D and R in the next 6 hours.

The problem is solved in multiple steps: First, deep learning-based probabilistic models are trained to predict the TC track and intensity in the next 6 hours; then, the wind speed V, rainfall intensity I, and water film depth (WFD) D at given locations of the road network and distribution lines are calculated using analytical or empirical models; lastly, the failure probabilities, the road capacity, and the free-flow travel speed are calculated using empirical models based on the predicted V, I, and D.

B. Dataset and Data Preprocessing

In this study, the TC track and intensity models were trained and evaluated on the CMA Tropical Cyclone Best Track Dataset [31], [32] obtained from the China Meteorological Administration (CMA). The dataset covers TCs developed over the western North Pacific and provides 6-hourly records for each TC. Each record contains the record date, TC name, center longitude, and latitude coordinates, intensity category, minimum central pressure, and two-minute mean maximum sustained wind speed near the TC center. The longitude, latitude and minimum central pressure were extracted from the dataset as the raw track data. A data cleaning process was performed to remove the extreme values (longitude $\lambda > 180°$ E, latitude $\phi > 55°$ N, or TC translation speed $c > 30m/s$) before constructing the input feature space for the model. The TC translation speed c was calculated using the Haversine formula:

$$a = \sin^2\left(\frac{\Delta\lambda}{2}\right) + \cos\lambda_1 \cdot \cos\lambda_2 \cdot \sin^2\left(\frac{\Delta\phi}{2}\right) \tag{1}$$

$$hav = 2 \cdot R \cdot \arctan\left(\sqrt{\frac{a}{1-a}}\right) \tag{2}$$

$$V = \frac{hav}{\Delta t} \tag{3}$$

To construct the input feature space, a set of common predictors selected by the climatology and persistence (CLIPER) model [33] were computed. A total of 26 input features were obtained (see Table I). The predictors are then normalized and split into training, validation, and test datasets with a ratio of 7:2:1.

C. Multitask Learning-based TC Track Forecast Model

The prediction of the TC track can be achieved using artificial neural networks (ANNs or NNs). NNs are layered machine learning models that mimic the way the human brain operates. A typical NN consist of an input layer, one or more hidden layers, and an output layer. Each layer has its associated activation function, which is usually a threshold function that determines if the nodes in this layer are activated. Like other machine learning models, NNs rely on training data to learn and improve their performance over time. For the deterministic TC track prediction task, which is a regression task, the NN model is usually trained by minimizing the mean square error (MSE) loss on the training data:

$$\theta^* = \underset{\theta}{\operatorname{argmin}}\, \mathcal{L}_\theta = \underset{\theta}{\operatorname{argmin}}\, \frac{1}{N}\sum_{i=1}^{N}(y_i - \hat{y}_i)^2 \tag{4}$$

where θ is the set of trainable parameters of the NN (including the neural network weights w and biases b), N is the total number of training data, y is the training target value, and $\hat{y}$ is the NN prediction.

However, for highly uncertain prediction tasks such as TC track prediction, we may also want to obtain the conditional probability distribution of future TC tracks. The prediction of the probability distribution can be achieved by combining an NN and a mixture model, resulting in an MDN. The mixture model consists of N_M mixture components which belong to a particular parametric distribution function. The mixture model can be expressed as a weighted sum of its components, and the weights add up to 1. For example, a Gaussian mixture model with K_M can be written as:

$$\mathcal{N}(y|\mu, \sigma) = \frac{1}{\sigma\sqrt{2\pi}} e^{-\frac{(y-\mu)^2}{2\sigma^2}} \tag{5}$$

$$p(y|x) = \sum_{i=1}^{K} \pi_i(x)\mathcal{N}_i(y|\mu_i(x), \sigma_i^2(x)) \tag{6}$$

$$\sum_{i=1}^{K_M} \pi_i = 1 \tag{7}$$

TABLE I
PREDICTORS USED BY THE PROPOSED MODEL

Predictor	Description
$x_1 - x_4$	Central pressure at current time, -6h, -12h, and -18h
$x_5 - x_8$	Longitude at current time, -6h, -12h, and -18h
$x_9 - x_{12}$	Latitude at current time, -6h, -12h, and -18h
$x_{13} - x_{16}$	Zonal motion at current time, -6h, -12h, and -18h
$x_{17} - x_{20}$	Meridional motion at current time, -6h, -12h, and -18h
$x_{21} - x_{23}$	Longitude difference of past 6h, 12h, and 18h
$x_{24} - x_{26}$	Latitude difference of past 6h, 12h, and 18h

where π_i is the mixture component weight and $p(y|x)$ denotes the conditional probability distribution of the output y given input x. The mixture model parameters, namely pi_i, μ_i, and σ_i, are predicted by an NN, and the mixture model works as the output layer in an MDN. To properly train an MDN model, the negative log-likelihood (NLL) loss is minimized on the training dataset:

$$\theta^*_{\text{MDN}} = \underset{\theta_{\text{MDN}}}{\operatorname{argmin}} \mathcal{L}_{\theta_{\text{MDN}}} = \underset{\theta_{\text{MDN}}}{\operatorname{argmin}} \sum_{i=1}^{N} -\log(y_i|x_i) \tag{8}$$

The deterministic and probabilistic TC track prediction models can be combined into one model to produce better-quality results by utilizing MTL. The different tasks in the MTL model share low-level hidden layer features to improve generalization ability. Each task also has its own task-specific layers and loss on top of the shared layers. The total loss of an MTL model is a weighted sum of the individual task losses. In this work, the MDN is employed to predict the probability distribution of the residual between the deterministic track prediction and the true values. Therefore, the total loss of the proposed MTL model $\mathcal{L}_{\theta_{\text{MTL}}}$ is given by:

$$\mathcal{L}_{\theta_{\text{MTL}}} = \alpha\mathcal{L}_{\text{Det}} + (1-\alpha)\mathcal{L}_{\text{Prob}} \tag{9}$$

$$\mathcal{L}_{\text{Det}} = \frac{1}{N}\sum_{i=1}^{N}(y_i - \hat{y}_i)^2 \tag{10}$$

$$\mathcal{L}_{\text{Prob}} = \sum_{i=1}^{N}\log(y_i - \hat{y}_i|x_i) \tag{11}$$

where $\mathcal{L}_{\text{Det}}$ is the deterministic prediction loss, $\mathcal{L}_{\text{Prob}}$ is the MDN prediction loss, $\hat{y}$ is the output of the deterministic prediction, α is a hyperparameter that denotes the weights of different loss terms, and x_i, y_i are from the training set $\{x_i, y_i\}_{i=1}^{N}$. To reduce the burden of hyperparameter tuning, the problem of predicting λ, lat, and p_c is solved using three different MTL models, respectively.

D. Forecast Model Training with Automatic Hyperparameter Tuning

The NN model performance is highly sensitive to hyperparameters. Manually adjusting the hyperparameters is very inefficient and time-consuming since you need to fully train the model every time you adjust the hyperparameters. Apart from the common hyperparameters of NN models, such as type of optimizer, learning rate, and batch size, the proposed MTL model has two unique hyperparameters that need to be tuned: the loss weights α and the number of mixture components K_M. In this work, two automatic hyperparameter tuning methods were developed to tune the two unique hyperparameters.

1) Uncertainty and Variance-based Automatic Loss Weighting: Uncertainty-based loss weights tuning was first proposed in [34]. Recently, the authors in [35] proposed a revised version of the uncertainty-based method. The original and revised uncertainty-based tuning strategies are proven to be effective in many applications. However, [36] made a comparison of different loss weighting strategies and suggested that for different tasks, the best strategies might be different. Therefore, in this work, we train the same model with different loss weighting strategies and preserve the trained model with the best test performance. The different strategies used in this work include the original and revised uncertainty-based strategies and a naive variance-based strategy. The naive variance-based strategy can be expressed as:

$$(\theta_{\text{MTL}}, \alpha)^* = \underset{\theta_{\text{MTL}},\alpha}{\operatorname{argmin}} \mathcal{L}_{\theta_{\text{MTL}},\alpha} \tag{12}$$

$$\mathcal{L}_{\theta_{\text{MTL}},\alpha} = \alpha\mathcal{L}_{\text{Det}} + (1-\alpha)\mathcal{L}_{\text{Prob}} + (\alpha\mathcal{L}_{\text{Det}} - \overline{\mathcal{L}})^2 + ((1-\alpha)\mathcal{L}_{\text{Prob}} - \overline{\mathcal{L}})^2 \tag{13}$$

$$\overline{\mathcal{L}} = \frac{\alpha\mathcal{L}_{\text{Det}} + (1-\alpha)\mathcal{L}_{\text{Prob}}}{2} \tag{14}$$

where $\overline{\mathcal{L}}$ represents the mean of the loss terms. The naive variance-based strategy just makes α a trainable parameter of the NN model and minimizes the loss term variance to avoid trivial values of α (i.e. 0 or 1).

2) Differntiable Hyperparameter Search for K_M: The differentiable architecture search (DARTS) was first proposed in [37]. DARTS enables gradient-based optimization of hyperparameters, which is significantly faster than the conventional evolutionary algorithm or reinforcement learning-based approaches. However, the original DARTS only works for convolutional neural networks (CNNs) or recurrent neural networks (RNNs). In this work, we developed a differentiable search method for the mixture model layer of the MDN. Similar to DARTS, a set of K_M values were selected as candidate operations which represents some function $o(\cdot)$ to be applied to the input of the mixture model. The DARTS algorithm requires that all the operations have the same input and output dimensions. Therefore, the operation for a

Algorithm 1: Training process of the proposed MTL model with automatic hyperparameter search.

Data: Training and validation dataset $\{x_{\text{tr},i}, y_{\text{tr},i}\}_{i=1}^{N_{\text{tr}}}$, $\{x_{\text{val},i}, y_{\text{val},i}\}_{i=1}^{N_{\text{val}}}$, untrained MTL model M parametrized by NN weights θ, and the set of candidate K_M values $\mathcal{K}$

Result: Trained neural network with weights θ^*

Replace the mixture model layer of M with a mixed operation based on $\mathcal{K}$ parameterized by w to get model M'.

Create 3 different models M_1, M_2, M_3 based on M' using the 3 loss functions described in section III-D1. These 3 models are essentially parameterized by $M_1 = (\theta_1, \alpha_1, w_1)$, $M_2 = (\theta_2, \alpha_2, w_2)$, and $M_3 = (\theta_3, \alpha_3, w_2)$.

foreach $M_i \in \{M_1, M_2, M_3\}$ **do**

  Set the initial learning rate $\xi_i \leftarrow \xi_i^0$ for the optimizer. Randomly initialize θ_i, α_i, and w_i.

  while $\mathcal{L}_{val}(\theta_i, \alpha_i, w_i)$ *is not converged* **do**

    Update w_i by descending $\nabla_{w_i}\mathcal{L}_{\text{val}}(\theta_i - \xi_i\nabla_{\theta_i}\mathcal{L}_{\text{tr}}(\theta_i, \alpha_i, w_i), \alpha_i - \xi\nabla_{\alpha_i}\mathcal{L}_{\text{tr}}(\theta_i, \alpha_i, w_i), w_i)$.

    Update θ_i, α_i by descending $\nabla_{\theta_i}\mathcal{L}_{\text{tr}}(\theta_i, \alpha_i, w_i)$.

  end

  $K_{M,i}^* \leftarrow \text{argmin}_{K_M \in \mathcal{K}}\, w_i^*$

end

$M'' \leftarrow \text{argmin}_{M_i \in \{M_1, M_2, M_3\}}\, \mathcal{L}_{\text{val}}(M_i)$. Set $K_M \leftarrow K_M''^*$ for the original model M and set the loss function of M to be the same as M''

Re-initialize θ and α, train M until validation loss converges. Save the weights of M as θ^*

particular K_M value is defined as a fully connected layer with identity activation followed by a mixture model layer with K_M mixture components. The fully connected layers in different operations ensure that the correct number of mixture parameters are created from the same input. The number of output dimensions of the mixture model layer is equal to the number of probabilistic predictions, which is identical for all operations. Once the operations are properly defined, a softmax over all the operations is applied to relax the search space to a continuous space. The different operations are weighted and summed up via element-wise concatenation. In this way, the weights of different operations can be optimized together with the NN weights. After the optimization, the operation with the maximum weight values is preserved as the search result.

The proposed training strategy is a combination of III-D1 and III-D2. The pseudocode of the proposed hyperparameter tuning strategy is presented in Algorithm 1.

E. Status of Distribution Lines and Highway Road Segments under TC Events

1) Precipitation and Wind Field Model: Once the proposed TC track models are properly trained, the prediction results of the models can be used for sampling precipitation and wind speed at given locations in an HTS during TC events. An empirical rainfall model [15] and a linear height-resolving wind field model [16] are employed to generate the rain rate and wind speed. The inputs of both models include central pressure, translation speed, radius to maximum winds, and storm track, which can all be obtained based on the track forecasting results.

2) Failure Status of Distribution Lines: The failure status of a distribution line is decided by the failure status of its components, namely towers and conductors. The tower failure probability calculation is based on fragility analysis [38]. First, the equivalent wind speed is computed based on wind speed and rainfall intensity. The failure probability $p_{tw,i}(t)$ of a transmission tower can then be calculated by a lognormal fragility curve [38], while considering the wind attacking angle [18]. The failure rate of a conductor segment is calculated using a Poisson regression-based model [19]. Since repair of the failure components is not considered during a TC event, the failure probability of towers and conductors also needs to be updated based on the failure status of previous time steps [39]. The towers and conductors along a distribution line are assumed to fail independently. The distribution line fails if at least one of its conductor segments or towers fails.

3) Road Capacity and Free-Flow Speed of Road Segments: For inundation-sensitive road segments, the free-flow travel time v_f and road capacity q_c are assumed to be affected by the rainfall and waterlogging on the road. To get v_f and q_c on highway road segments, the water film depth (WFD) is computed using an analytical model [17] based on the road segment location and predicted rainfall described in III-E1. Then, the empirical models described in [40] are employed to calculate v_f and q_c based on the WFD and rainfall prediction on road segments.

IV. Resilience Assessment Problem for Self-Sustained HTSs

This section presents a two-stage resilience assessment model for self-sustained HTSs. The uncertainty factors (i.e., wind power, line status, road capacities, and free-flow speeds) obtained in the previous section are considered in this model. The resilience assessment is modeled based on the integrated problem of dynamic traffic assignment and optimal power flow (OPF) [22]. The problem is formulated as a two-stage economic dispatch problem [23] integrated with a two-stage distributionally robust optimization (DRO) framework [27]. The two-stage model is presented in subsections A and B. Then, the DRO framework is depicted in part C. In part D, the solution method based on the mixed integer linear programming (MILP) reformulation is introduced.

A. First-stage Optimization

The first stage minimizes the total travel time of the vehicles and the costs of generation and reserves based on the

uncertainty factors, as follows:

$$\min \sum_{s\in\mathcal{N}_S}\sum_{a\in\mathcal{A}/\mathcal{A}_S}\sum_{t\in\mathcal{T}}\sum_{tc\in\mathcal{C}}\sum_{e\in\mathcal{E}_c} f_{\text{TT}}\delta_a\left[U_{a,c}^{s,e}(t)-V_{a,c}^{s,e}(t)\right] + \sum_{t\in\mathcal{T}}\sum_{g\in\mathcal{G}}\{f_g P_g(t)\delta+[f_g^{\text{R}}R_g(t)+f_g^{r,+}r_g^{+}(t)+f_g^{r,-}r_g^{-}(t)]\delta\} \tag{15}$$

$$\text{s.t.} \quad \sum_{d\in\mathcal{D}}P_d(t)+\sum_{ji}P_{ji}(t)+\sum_{c\in\mathcal{C}_j}P_c^{\text{ev}}(t) = \sum_{ij}P_{ij}(t)+\sum_{g\in\mathcal{G}}P_g(t)+\sum_{w\in\mathcal{W}}P_w(t),\forall t,j \tag{16}$$

$$P_c^{\text{ev}}(t)=\sum_{a\in M(c)}\sum_{s\in\mathcal{N}_S}\sum_{e\in\mathcal{E}_c}P_a^{\text{ev}}\left[U_{a,c}^{s,e}(t)-V_{a,c}^{s,e}(t)\right], \quad \forall c\in\mathcal{C},t \tag{17}$$

The power balance constraint is given by Eqn. (16). The EV interaction is represented by Eqn. (17), where $M(c)$ is the mapping from the charging station set to the charging link set.

B. Second-stage Optimization

Based on the real value of the uncertainty factors, the generation $p_g(t)$, and EV interaction $p_c^{\text{ev}}(t)$ are re-dispatched to minimize the unmet traffic demand $D_{a,s}^{\text{ud}}(t)$, load shedding $p_d^{\text{ls}}(t)$, curtailment of generation $p_g^{\text{gc}}(t)$, and wind power $p_w^{\text{wc}}(t)$ in the second stage, as follows:

$$\min \sum_{s\in\mathcal{N}_S}\sum_{t\in\mathcal{T}}\sum_{a\in\mathcal{A}_S}f_{\text{VOUD}}D_{a,s}^{\text{ud}}(t)+\sum_{t\in\mathcal{T}}\sum_{d\in\mathcal{D}}f_{\text{VOLL}}p_d^{\text{ls}}(t)\delta + \sum_{t\in\mathcal{T}}\sum_{g\in\mathcal{G}}f_{\text{VOGC}}p_g^{\text{gc}}(t)\delta+\sum_{t\in\mathcal{T}}\sum_{w\in\mathcal{W}}f_{\text{VOWC}}p_w^{\text{wc}}(t)\delta \tag{18}$$

$$\text{s.t.} \quad \sum_{c\in\mathcal{C}}\sum_{e\in\mathcal{E}}u_{a,c}^{s,e}(t)+D_{a,s}^{\text{ud}}(t) = D_{a,s}(t)+\Delta D_{a,s}(t),\forall a\in\mathcal{A}_R,s,t \tag{19}$$

$$u_{a,c}^{s,e}(t)=U_{a,c}^{s,e}(t),\forall a\in\mathcal{A}/\mathcal{A}_{\text{C}},c,s,e,t \tag{20}$$

$$v_{a,c}^{s,e}(t)=V_{a,c}^{s,e}(t),\forall a\in\mathcal{A}/\mathcal{A}_{\text{C}},c,s,e,t \tag{21}$$

$$\sum_{s\in\mathcal{N}_S}\sum_{c\in\mathcal{C}}\sum_{e\in\mathcal{E}}[v_{a,c}^{s,e}-u_{a,c}^{s,e}(t-t_a)]\le 0, \quad \forall a\in\mathcal{A}/\mathcal{A}_{\text{C}},t \tag{22}$$

$$\sum_{s\in\mathcal{N}_S}\sum_{c\in\mathcal{C}}\sum_{e\in\mathcal{E}}[u_{a,c}^{s,e}(t)-v_{a,c}^{s,e}(t-\beta_a)]\le L_a k_{\text{jam}}, \quad \forall a\in\mathcal{A}/\mathcal{A}_{\text{C}},t \tag{23}$$

$$\sum_{ji}p_{ji}(t)-\sum_{ij}p_{ij}(t)=\sum_{w\in\mathcal{W}_j}[P_w(t)+\Delta p_d(t)-p_w^{\text{wc}}(t)] + \sum_{g\in\mathcal{G}_j}[p_g(t)-p_g^{\text{gc}}(t)]-\sum_{d\in\mathcal{D}_j}[P_d(t)+\Delta p_d(t)-p_d^{\text{ls}}(t)] - \sum_{c\in\mathcal{C}_j}p_c^{\text{ev}}(t),\forall t,j \tag{24}$$

$$p_c^{\text{ev}}(t)=\sum_{a\in M(c)}\sum_{s\in\mathcal{N}_S}\sum_{e\in\mathcal{E}_c}p_a^{ev}\left[u_{a,c}^{s,e}(t)-v_{a,c}^{s,e}(t)\right], \quad \forall c\in\mathcal{C},t \tag{25}$$

$$(I_{ij}(t)-1)M\le p_{ij}(t)-B_{ij}(\gamma_i(t)-\gamma_j(t))\le(1-I_{ij}(t))M,\forall t,ij \tag{26}$$

Constraint (19) defines the unmet traffic demand. The real traffic flow is depicted by Eqn. (20)-(21). The free-flow travel time and the backward waves travel time are limited by Eqn. (22)-(23). Constraint (24) relaxes the power balance constraint to realize load shedding. The second-stage EV interaction is represented by Eqn. (25). The impact of line failure on power flow is represented by (26). For more details of the two-stage problem constraints, please refer to [22], [23], [27].

C. DRO Formulation

The resilience assessment problem is formulated as the following two-stage distributionally robust optimization problem:

$$\min_{\mathbf{x}\in\mathbf{X}} \ \mathbf{c}^{\text{T}}\mathbf{x}+\rho\max_{\mathbb{P}\in\mathcal{P}}\{\mathbb{E}[Q_{\text{DRO}}(\mathbf{x},\boldsymbol{\xi})] + (1-\rho)C_{\text{VaR},\beta}[Q_{\text{DRO}}(\mathbf{x},\boldsymbol{\xi})]\} \tag{27}$$

$$Q_{\text{DRO}}(\mathbf{x},\boldsymbol{\xi})=\min_{\mathbf{y}\in\mathbf{Y}}\mathbf{d}^{\text{T}}\mathbf{y} \tag{28}$$

where $\mathbf{c}$ and $\mathbf{x}$ are the decision variables and cost coefficients of the first stage, $\mathbf{y}$ and $\mathbf{d}$ are the second-stage decision variables, and the cost coefficients, $\boldsymbol{\xi}$ is the vector of uncertain variables, $C_{\text{VaR},\beta}$ represents the conditional value at risk (CVaR) under confidence level β, ρ is a risk aversion factor, and $\mathcal{P}$ is the ambiguity set

$$\mathcal{P}=\left\{\mathbb{P}:\sum_{\omega\in\Omega}|\pi_\omega^0-\pi_\omega|\le\tau_{\text{DRO}}\right\} \tag{29}$$

where π_ω^0 and π_ω are the discrete probabilities responding to the scenario ω in nominal and true distribution, τ_{DRO} is the total variation distance threshold, and Ω is a probability space with finite scenarios, whose empirical probability distribution could be estimated by non-parametric estimation.

D. Solution Methods

To solve the problem (27), the Lagrangian dual method is adopted in this work. Problem (27) is reformulated into the following MILP problem [41]:

$$\min \mathbf{c}^{\text{T}}\mathbf{x}+\tau_{\text{DRO}}z+(1-\rho)\eta+\sum_{\omega\in\Omega}\pi_\omega^0(z_\omega^+-z_\omega^-)+\vartheta \tag{30}$$

$$\text{s.t.} \quad \mathbf{G}\mathbf{x}+\mathbf{W}\mathbf{y}_\omega\ge\mathbf{h}-\mathbf{M}\boldsymbol{\xi}_\omega,\forall\omega\in\Omega \tag{31}$$

$$\mathbf{d}_\omega^{\text{T}}\mathbf{y}_\omega+\frac{1-\rho}{1-\beta_{\text{DRO}}}v_\omega\le z_\omega^+-z_\omega^-+\vartheta,\forall\omega\in\Omega \tag{32}$$

$$z_\omega^++z_\omega^--z\le 0,\forall\omega\in\Omega \tag{33}$$

$$\mathbf{d}_\omega^{\text{T}}\mathbf{y}_\omega-\eta\le v_\omega,\forall\omega\in\Omega \tag{34}$$

$$z,z_\omega^+,z_\omega^-,v_\omega\ge 0 \tag{35}$$

where $z,\vartheta,z_\omega^+,z_\omega^-,v_\omega$ are auxiliary variables. η is the value-at-risk (VaR) of $Q_{\text{DRO}}(\mathbf{x},\boldsymbol{\xi})$ corresponding to confidence level β_{DRO}. This MILP problem is solved by Gurobi in this work.

V. Case Studies

The performance of the probabilistic TC track models is hard to evaluate solely based on the resilience assessment results. Therefore, in this section, we first evaluate the performance of the proposed MTL models against statistical models in subsection A. In subsection B, the proposed resilience assessment problem is studied under different cases.

TABLE II
NLL AND PI EVALUATION RESULTS

		NLL	PI-based Accuracy	Mean PI Length
Longitude	MLR	2152.1368	94.63%	1.5040
	Trivial MTL	1159.7517	94.79%	1.3542
	Proposed MTL	**1102.7261**	**94.98%**	1.3545
Latitude	MLR	1036.4191	94.81%	1.1941
	Trivial MTL	144.8669	95.35%	1.1326
	Proposed MTL	**122.4152**	**95.72%**	1.1107
Intensity	MLR	13287.4320	94.69%	14.7657
	Trivial MTL	141.7534	93.11%	14.4262
	Proposed MTL	**-3372.3504**	**94.86%**	14.4879

A. TC Track Models

1) Case Description: The proposed TC track models are tested against the following models:

- MLR: Multiple linear regression (MLR) models with normally distributed random error terms. The MLR coefficients and the normal distribution parameters are obtained by fitting the models with the same training dataset as the proposed model.
- Trivial MTL: MTL models with the same architecture as the proposed model but trained with trivial hyperparameters. The trivial weights are set to be 1 for all the loss terms and the number of mixture components is fixed at 64.

The set of candidate K_M values of the proposed model is set to be $\{16, 32, 64, 128, 256, 512\}$. In each case, 3 different models are trained for longitude, latitude, and central pressure, respectively. The neural network models are implemented and trained using Tensorflow[42] on a machine equipped with an NVIDIA GeForce RTX 3090 GPU.

2) Evaluation Metrics: NLL and prediction interval (PI) are used for evaluating the performance of the probabilistic prediction models. PI is a common tool to evaluate model prediction uncertainty with a given probability. PI gives a range within which the model is reasonably sure that the future observation lies. The given probability describes the sureness of the model about a certain PI. In this study, we evaluate the models using 95% PI. While the PI of the normal distribution is easy to calculate, the PI of the mixture model can not be calculated directly. In this work, the PI of the mixture model is estimated by solving for the 2.5% and 97.5% percentile based on the cumulative distribution function of the mixture model using Brent's method [43].

The NLLs and PIs of the models are evaluated on the test dataset. We propose the following 2 metrics based on the PIs:

- PI-based Accuracy: If the observed test data is within 95% PI, the probabilistic prediction is considered correct. The PI-based accuracy is then defined as the number of correctly predicted test cases divided by the total number of test cases.
- PI Length: For probabilistic prediction models, a wider PI indicates higher uncertainty. The model is preferable if it can capture the unseen observations with a smaller PI length. For MLR models, since the distribution of the residual term is fixed, the PI length is a fixed value. For the proposed model, the PI lengths depend on the input TC conditions.

3) Evaluation Results: Table II shows the evaluation results of the models. The NLL of the MTL models is significantly lower than that of the MLR models. While the longitude and latitude NLLs of the trivial MTL and the proposed MTL are similar, the proposed MTL has a significantly lower NLL on intensity prediction than that of the trivial MTL. The intensity forecasting is known to be much harder than the longitude and latitude prediction [11]. Therefore the intensity models are harder to train properly. The proposed MTL yields much lower NLL than the trivial MTL, indicating that the proposed training strategy is more effective for more complex models. Overall, the proposed MTL yields the lowest NLL in probabilistic predictions.

Table II also shows that the proposed MTL has the highest PI-based accuracy among all three tasks. The PI lengths of the MTL models are also smaller than the MLR models. To further investigate the predictive ability of the proposed models, the violin plots of the PI lengths of the MLR and proposed MTL models are plotted in Fig. 2. The plots indicate that the proposed MTL model has obviously more narrow PIs for longitude and latitude predictions. The distribution of the intensity PI lengths has two peaks: one above and one below the MLR PI length. This can be explained by plotting the PI lengths for a specific test TC (Fig. 3). While the mean PI lengths of the proposed MTL model is smaller than that of the MLR model, the PI lengths of the proposed MTL model get larger when the target values have larger fluctuations, accounting for larger uncertainties. The proposed model does a better job of capturing the uncertainties in TC track predictions than the conventional statistical models.

B. Resilience Assessment

1) Case Description: To assess the effectiveness of the proposed resilience assessment scheme for self-sustained HTSs under TC events, a modified IEEE-14 test system with 2 wind farms (WFs) and a 14-node transportation network with 4

charging stations are employed for simulations. All the system parameters can be accessed online [44]. The following three cases are studied under 20 predicted scenarios:

- Case 1: The uncertain TC-related parameters are predicted by the MLR model, and EVs only work as charging loads.
- Case 2: The uncertain TC-related parameters are predicted by the proposed MTL model, and the EVs only work as charging loads.
- Case 3: The uncertain TC-related parameters are predicted by the proposed MTL model, and the EVs can be both charging loads and mobile energy storage, i.e. both the charging and discharging of the EVs are considered.

The input initial TC conditions are from the test data set. The obtained first-stage decisions of the three cases are then simulated under 80 scenarios generated by the proposed MTL model.

TABLE III
RESULTS UNDER THE GIVEN FIRST STAGE DECISION IN CASES 1-3

Case	Expected total cost ($)	Total cost under ξ^* ($)
1	521240	708740
2	498560	771100
3	498810	761460

2) Assessment Results: As listed in Table III, the expected cost in Case 2 is 22680$ lower than that in Case 1. The cumulative density function (CDF) of the total cost is plotted in Fig. 4. In the scenarios with a probability of less than 0.05%, the cost in Case 2 is higher than in Case 1. The maximum cost in Case 2 is 62360$ higher. Compared with Case 2, although the expected cost in Case 3 is increased by 250$, the costs are reduced in scenarios with the probability of 0.1%, and the maximum cost is reduced by 9640$. Results indicate that more accurate forecasting data may reduce costs in most scenarios. In addition, although the expected cost increases when EVs are treated as mobile energy storage resources, the costs in extreme scenarios may decrease.

The results of unmet traffic demand are illustrated in Fig. 5. As seen in Fig. 5, the unmet traffic demand in Case 2 is the lowest. This is because the mean free-flow time predicted by

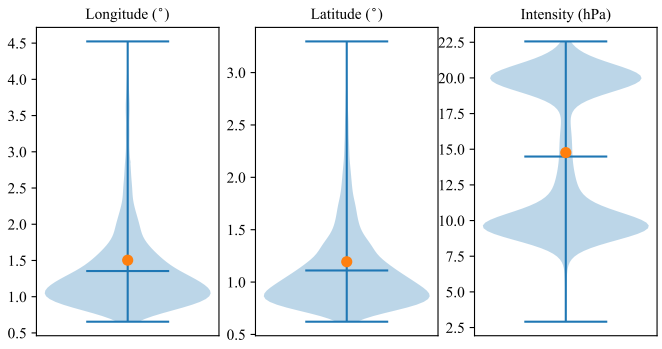

Fig. 2. PI lengths of the MLR and proposed MTL models. The red dots are the PIs of the MLR models.

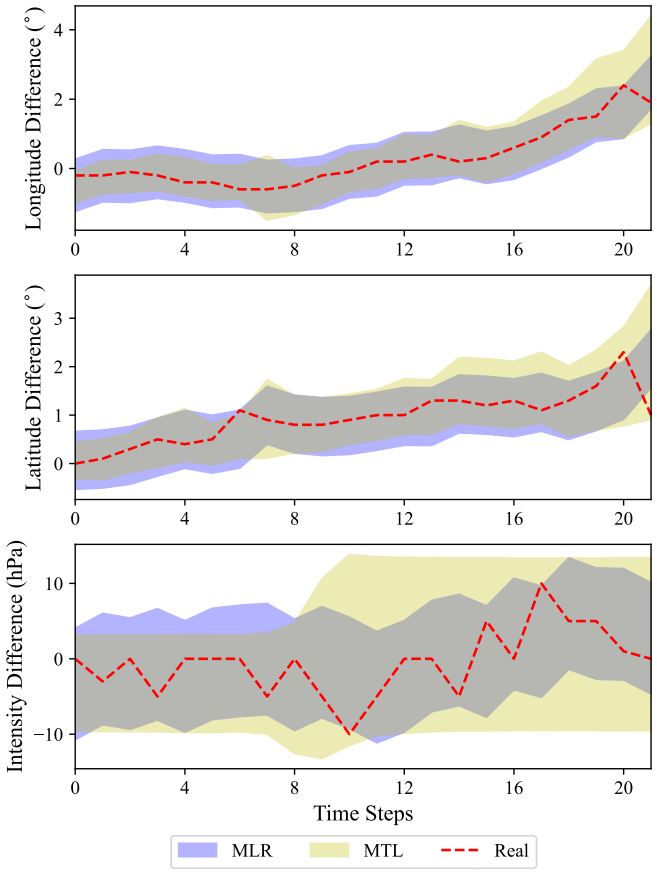

Fig. 3. PIs of the MLR and proposed MTL models for a test TC.

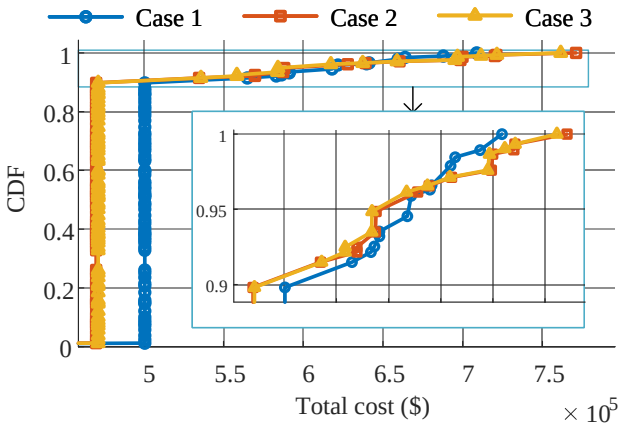

Fig. 4. Cumulative probability density function of total costs under the given first stage decision in Cases 1-3

the proposed MTL model is less than, and the road capacities are larger than those obtained by the MLR model. The unmet traffic demand in Case 3 is more than that in Case 2. The reason is that the charging of 120 vehicles cannot be satisfied due to limited charging piles and the long interaction time of EVs as energy storage resources.

The results of load shedding are illustrated in Fig. 6. As seen in Fig. 6, load shedding occurs in 5 scenarios in Case 1. In Case 1, the generators in time slot 15 are set to 240MW

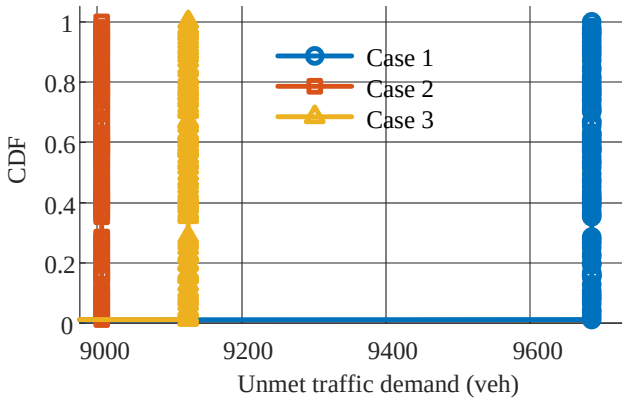

Fig. 5. Cumulative probability density function of unmet traffic demand under the given first stage decision in Cases 1-3

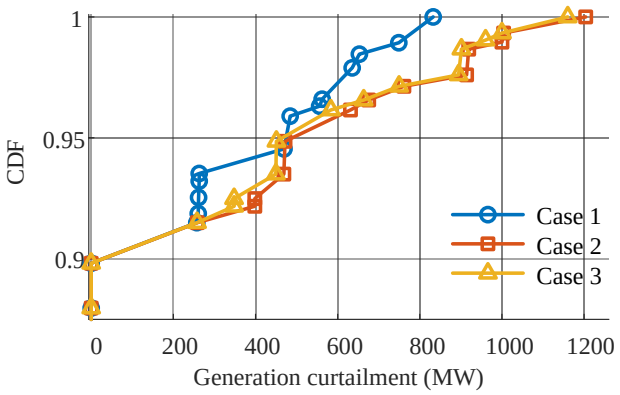

Fig. 7. Cumulative probability density function of generation curtailment under the given first stage decision in Cases 1-3

under the 215MW expected wind power obtained by the MLR model, which is not enough in these 5 scenarios with less wind power. In Cases 2 and 3, the generator outputs are set to 450MW under the 16MW expected wind power obtained by the proposed MTL model, which is enough for the power load. Thus there can be 0 load shedding in Cases 2 and 3.

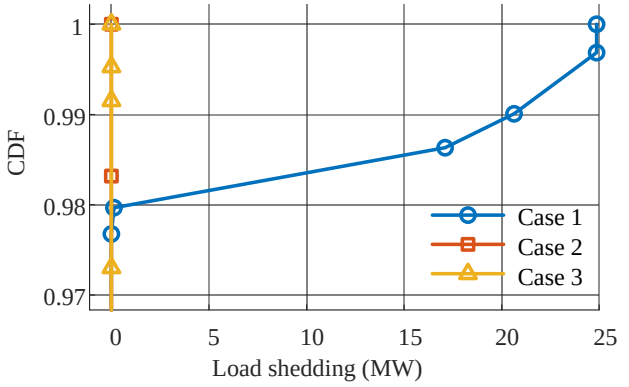

Fig. 6. Cumulative probability density function of load shedding under the given first stage decision in Cases 1-3

The results of generation curtailment are shown in Fig. 7. As seen in Fig. 7, generation curtailment in Case 1 is the lowest while that in Case 2 is the highest in scenarios with a probability of 0.08% scenarios. The wind power is high in these scenarios. Since the set point is higher in Case 2, the generation curtailment is larger. In comparison with Case 2, EVs as energy storage can reduce the generation curtailment by charging under high wind power and discharging under low wind power.

This case study results suggest that the total cost can be reduced if the TC prediction is more accurate. For the selected TC initial condition, the 95% prediction intervals of case 1 and case 2 models are [936.93 hPa, 964.18 hPa] and [936.10 hPa, 950.86 hPa], respectively. The real value is 955 hPa. Therefore, the MLR model in this specific case always underestimates the central pressure, resulting in lower travel speed and road capacity prediction values. Therefore, in most scenarios, the total cost in case 1 is higher than in case 2.

VI. Conclusion

The resilience assessment problem for HTSs under EWEs is addressed in this paper. An MTL-based probabilistic prediction model is proposed to assess the impact of TC events. The proposed MTL model is trained using a novel automatic hyperparameter searching algorithm to avoid manual hyperparameter tuning. A proactive resilience assessment scheme is formulated as a two-stage distributionally robust optimization problem, which considers the self-sustainability of HTSs as a joint emergency management problem. The proposed MTL model is tested against statistical models, while the proposed resilience assessment scheme is verified by simulation on a system consisting of a modified IEEE-14 test system with 2 WFs and a 14-node transportation network. The main conclusions include:

- The proposed MTL model outperforms statistical models in probabilistic prediction tasks. The conditional probability density prediction ability and variable length prediction interval of the proposed model allow for more accurate modeling of the TC uncertainty.
- The hyperparameters of the proposed MTL model can be automatically tuned using the proposed hyperparameter search method. The performance of the MTL model trained using the proposed hyperparameter search method is better than the MTL model trained using trivial hyperparameters, especially when the prediction problem is harder.
- The resilience levels of self-sustained HTSs under different modes can be quantified by the proposed resilience assessment scheme. The simulation results show that the more accurate EWE prediction models and using EVs as a mobile energy storage system can reduce the total cost of the proposed resilience assessment scheme.

References

[1] y. Wang, "Learning from others: Energy utilization of foreign highway construction," *Transport Construction & Management*, vol. 2, pp. 42–45, 2018.

[2] H. Murakami, E. Levin *et al.*, "Dominant effect of relative tropical atlantic warming on major hurricane occurrence," *Science*, vol. 362, no. 6416, pp. 794–799, 2018.

[3] R. Seidl, D. Thom *et al.*, "Forest disturbances under climate change," *Nature climate change*, vol. 7, no. 6, pp. 395–402, 2017.

[4] S. Ahmed and K. Dey, "Resilience modeling concepts in transportation systems: A comprehensive review based on mode, and modeling techniques," *Journal of Infrastructure Preservation and Resilience*, vol. 1, no. 1, p. 8, Dec. 2020.

[5] J. Côté, S. Gravel *et al.*, "The operational cmc–mrb global environmental multiscale (gem) model. part i: Design considerations and formulation," *Monthly Weather Review*, vol. 126, no. 6, pp. 1373–1395, 1998.

[6] T. N. Krishnamurti, C. Kishtawal *et al.*, "Multimodel ensemble forecasts for weather and seasonal climate," *Journal of Climate*, vol. 13, no. 23, pp. 4196–4216, 2000.

[7] L. R. Russell, "Probability distributions for hurricane effects," *Journal of the Waterways, Harbors and Coastal Engineering Division*, vol. 97, no. 1, pp. 139–154, 1971.

[8] P. J. Vickery and L. A. Twisdale, "Prediction of Hurricane Wind Speeds in the United States," *Journal of Structural Engineering*, vol. 121, no. 11, pp. 1691–1699, Nov. 1995.

[9] P. J. Vickery, P. F. Skerlj, and L. A. Twisdale, "Simulation of Hurricane Risk in the U.S. Using Empirical Track Model," *Journal of Structural Engineering*, vol. 126, no. 10, pp. 1222–1237, Oct. 2000.

[10] S. Zhang and K. Nishijima, "Statistics-based investigation on typhoon transition modeling," in *Proc. Seventh Int. Colloquium on Bluff Body Aerodynamics and Application*, 2012, pp. 364–373.

[11] R. Snaiki and T. Wu, "Revisiting hurricane track model for wind risk assessment," *Structural Safety*, vol. 87, p. 102003, Nov. 2020.

[12] S. Alemany, J. Beltran *et al.*, "Predicting Hurricane Trajectories Using a Recurrent Neural Network," *Proceedings of the AAAI Conference on Artificial Intelligence*, vol. 33, no. 01, pp. 468–475, Jul. 2019.

[13] F. Hao, L. Dou, and J. Jin, "Mixture Density Networks for Tropical Cyclone Tracks Prediction in South China Sea," *2021 International Joint Conference on Neural Networks (IJCNN)*, pp. 1–8, 2021.

[14] W. Qin, J. Tang *et al.*, "A typhoon trajectory prediction model based on multimodal and multitask learning," *Applied Soft Computing*, vol. 122, p. 108804, Jun. 2022.

[15] K. M. Geoghegan, P. Fitzpatrick *et al.*, "Evaluation of a synthetic rainfall model, P-CLIPER, for use in coastal flood modeling," *Natural Hazards*, vol. 92, no. 2, pp. 699–726, Jun. 2018.

[16] R. Snaiki and T. Wu, "A linear height-resolving wind field model for tropical cyclone boundary layer," *Journal of Wind Engineering and Industrial Aerodynamics*, vol. 171, pp. 248–260, Dec. 2017.

[17] J. Luo, J. Liu, and Y. Wang, "Validation Test on Pavement Water Film Depth Prediction Model," *China Journal of Highway and Transport*, vol. 28, no. 12, pp. 57–63, 2015.

[18] X. Fu, H.-N. Li, and G. Li, "Fragility analysis and estimation of collapse status for transmission tower subjected to wind and rain loads," *Structural Safety*, vol. 58, pp. 1–10, 2016.

[19] F. Xiao, J. D. McCalley *et al.*, "Contingency probability estimation using weather and geographical data for on-line security assessment," in *2006 International Conference on Probabilistic Methods Applied to Power Systems*. IEEE, 2006, pp. 1–7.

[20] W. Zhang, R. Li *et al.*, "Impact Analysis of Rainfall on Traffic Flow Characteristics in Beijing," *International Journal of Intelligent Transportation Systems Research*, vol. 17, no. 2, pp. 150–160, May 2019.

[21] X. Ni, H. Huang *et al.*, "Effect of heavy rainstorm and rain-induced waterlogging on traffic flow on urban road sections: Integrated experiment and simulation study," *Journal of Transportation Engineering, Part A: Systems*, vol. 147, no. 10, p. 04021057, 2021.

[22] H. Wang, Y.-P. Fang, and E. Zio, "Resilience-oriented optimal post-disruption reconfiguration for coupled traffic-power systems," *Reliability Engineering & System Safety*, vol. 222, p. 108408, 2022.

[23] B. D. Chung, T. Yao, and B. Zhang, "Dynamic traffic assignment under uncertainty: a distributional robust chance-constrained approach," *Networks and Spatial Economics*, vol. 12, no. 1, pp. 167–181, 2012.

[24] I. Yperman, "The link transmission model for dynamic network loading," Ph.D. dissertation, Katholieke Universiteit Leuven, 2007.

[25] Y. Hu, Y. Li, and J. Zheng, "Resilience-constrained economic dispatch for cascading failures prevention," in *2021 IEEE Sustainable Power and Energy Conference (iSPEC)*. IEEE, 2021, pp. 1692–1697.

[26] A. Lorca and X. A. Sun, "Adaptive robust optimization with dynamic uncertainty sets for multi-period economic dispatch under significant wind," *IEEE Transactions on Power Systems*, vol. 30, no. 4, pp. 1702–1713, 2014.

[27] C. Yang, W. Sun *et al.*, "Risk-averse two-stage distributionally robust economic dispatch model under uncertain renewable energy," *CSEE Journal of Power and Energy Systems*, 2021.

[28] I. E. Agency, "Co2 emissions from fuel combustion highlights," *Retrieved April*, vol. 22, p. 2012, 2011.

[29] Y. Wei, B. Yu *et al.*, "Roadmap for achieving china's carbon peak and carbon neutrality pathway," *Journal of Beijing Institute of Technology (Social Science Edition)*, vol. 24, no. S20221165, p. 13, 2022.

[30] ""14th five-year" national key research plan "transportation infrastructure" key special application guide for 2021 projects," http://www.chinazx.org.cn/i.php?id=3421.

[31] M. Ying, W. Zhang *et al.*, "An overview of the china meteorological administration tropical cyclone database," *Journal of Atmospheric and Oceanic Technology*, vol. 31, no. 2, pp. 287–301, 2014.

[32] X. Lu, H. Yu *et al.*, "Western north pacific tropical cyclone database created by the china meteorological administration," *Advances in Atmospheric Sciences*, vol. 38, no. 4, pp. 690–699, 2021.

[33] J. A. Knaff, M. DeMaria *et al.*, "Statistical, 5-Day Tropical Cyclone Intensity Forecasts Derived from Climatology and Persistence," *Weather and Forecasting*, vol. 18, no. 1, pp. 80–92, Feb. 2003.

[34] R. Cipolla, Y. Gal, and A. Kendall, "Multi-task Learning Using Uncertainty to Weigh Losses for Scene Geometry and Semantics," in *2018 IEEE/CVF Conference on Computer Vision and Pattern Recognition*. Salt Lake City, UT, USA: IEEE, Jun. 2018, pp. 7482–7491.

[35] L. Liebel and M. Körner, "Auxiliary Tasks in Multi-task Learning," May 2018.

[36] T. Gong, T. Lee *et al.*, "A Comparison of Loss Weighting Strategies for Multi task Learning in Deep Neural Networks," *IEEE Access*, vol. 7, pp. 141 627–141 632, 2019.

[37] H. Liu, K. Simonyan, and Y. Yang, "DARTS: Differentiable Architecture Search," *arXiv:1806.09055 [cs, stat]*, Apr. 2019.

[38] M. Ouyang and L. Dueñas-Osorio, "Multi-dimensional hurricane resilience assessment of electric power systems," *Structural Safety*, vol. 48, pp. 15–24, May 2014.

[39] Y. Liu and C. Singh, "A methodology for evaluation of hurricane impact on composite power system reliability," *IEEE Transactions on Power Systems*, vol. 26, no. 1, pp. 145–152, 2010.

[40] X. Ni, H. Huang *et al.*, "Study of Local Traffic Flow Fluctuation under Rainfall and Waterlogging with Characteristics of Dynamic Spatiotemporal Changes," *Journal of Transportation Engineering, Part A: Systems*, vol. 148, no. 7, p. 04022039, Jul. 2022.

[41] R. Huang, S. Qu *et al.*, "Data-driven two-stage distributionally robust optimization with risk aversion," *Applied Soft Computing*, vol. 87, p. 105978, 2020.

[42] M. Abadi, A. Agarwal *et al.*, "TensorFlow: Large-scale machine learning on heterogeneous systems," Software available from tensorflow.org, Tech. Rep., 2015. [Online]. Available: https://www.tensorflow.org/

[43] R. P. Brent, *Algorithms for minimization without derivatives*. Courier Corporation, 2013.

[44] H. Yan, "Parameters of self-sustained highway transportation systems." 2023. [Online]. Available: https://dx.doi.org/10.21227/c8xx-3v17